The Probe Rules in Single Particle Tracking

Mathias P. Clausen and B. Christoffer Lagerholm*

Department of Physics and Chemistry, and MEMPHYS – Center for Biomembrane Physics, University of Southern Denmark, Campusvej 55, DK-5230 Odense M, Denmark

Abstract: Single particle tracking (SPT) enables light microscopy at a sub-diffraction limited spatial resolution by a combination of imaging at low molecular labeling densities and computational image processing. SPT and related single molecule imaging techniques have found a rapidly expanded use within the life sciences. This expanded use is due to an increased demand and requisite for developing a comprehensive understanding of the spatial dynamics of bio-molecular interactions at a spatial scale that is equivalent to the size of the molecules themselves, as well as by the emergence of new imaging techniques and probes that have made historically very demanding and specialized bio-imaging techniques more easily accessible and achievable. SPT has in particular found extensive use for analyzing the molecular organization of biological membranes. From these and other studies using complementary techniques it has been determined that the organization of native plasma membranes is heterogeneous over a very large range of spatial and temporal scales. The observed heterogeneities in the organization have the practical consequence that the SPT results in investigations of native plasma membranes are time dependent. Furthermore, because the accessible time dynamics, and also the spatial resolution, in an SPT experiment is mainly dependent on the luminous brightness and photostability of the particular SPT probe that is used, available SPT results are ultimately dependent on the SPT probes. The focus of this review is on the impact that the SPT probe has on the experimental results in SPT.

Keywords: Diffusion, domains, dyes, gold particles, lateral dynamics, plasma membrane organization, quantum dots, single molecule imaging.

1. INTRODUCTION

The molecular composition and organization of the mammalian plasma membrane is very complex [1-9]. Hundreds if not thousands of different lipid species are present in the plasma membrane with the main lipid types being phospholipids (with a variety of fatty acid chain lengths and degrees of unsaturation), cholesterol, and sphingolipids. Phospholipids and cholesterol are present in about equal amounts and together account for 85-90 % of the total lipids while sphingolipids account for a large majority of the remaining lipids [10]. It has further been estimated that ~30 % of the genome in eukaryotic organisms encodes for membrane inserted and membrane associated proteins giving rise to thousands of different membrane protein species, many of which are present in the plasma membrane [11]. The relative proportion of lipids and membrane proteins in the plasma membrane has been shown to be approximately equal by weight, corresponding to about one protein per 50 lipids [12]. However, while the general features of the composition are well characterized, the molecular organization of the plasma membrane of mammalian cells is not known [1-4]. Much controversy exists in particular about the existence of lipid rafts, lipid-stabilized nanodomains which are thought to be highly enriched in cholesterol, glycosphingolipids (GSLs), and a wide variety of membrane proteins (e.g. glucosyl-phosphatidyl-inositol (GPI) anchored proteins) that are important for a range of cell signaling pathways [3, 5]. There are also other complementary models for the nanoorganization of the plasma membrane of cells that still remain to be fully evaluated [2, 7]. These include for example the anchored-transmembrane-picket-model, where the long-range lateral diffusion of membrane proteins and lipids in native plasma membranes is hindered by integral membrane proteins that are immobilized by direct interaction with the actin cytoskeleton [8].

The biggest challenge in studies of the molecular organization of the plasma membrane has been, and still is, the lack of experimental techniques that are capable of directly resolving possible small transient structures in the plane of the plasma membrane. The methods of choice to date have been the closely related single particle tracking (SPT) and single molecule fluorescent tracking (SMFT) imaging techniques. In both of these techniques information about the molecular organization of the plasma membrane is inferred from careful analysis of the motion of single lipids and membrane proteins that are embedded in the plasma membrane. Because SPT and SMFT are closely related imaging techniques, differing primarily only in the identity of the probe that has been attached to the target molecules, where for SPT the probe is composed of a particle (e.g. a gold particle, a fluorescent bead, or a fluorescent quantum dot (QD)) and for SMFT the probe is composed of a fluorescent dye or a fluorescent protein (FP), we will henceforth use the acronym SPT to refer to both.

As mentioned above, the organization of the native plasma membrane deviates significantly from that of simple,

*Address correspondence to this author at the Department of Physics and Chemistry, and MEMPHYS – Center for Biomembrane Physics, University of Southern Denmark, Campusvej 55, DK-5230 Odense M, Denmark; Tel: +45 6550 3505; Fax: +45 6550 4048; E-mail: lagerholm@memphys.sdu.dk

1389-2037/11 $58.00+.00

homogenous artificial model membranes. In fact, SPT experiments suggest that the native plasma membrane contains a variety of barriers that limits the motion of lipids and membrane proteins over a wide range of sizes, from tens to hundreds of nanometers, and durations, from a few milliseconds to seconds [8]. Consequently, in SPT experiments in native plasma membranes, there is an intricate relationship between the optical characteristics of the SPT probe and the accessible temporal sampling, the duration of an experiment, the spatial resolution, the results, and the interpretation of the results. This is because the brighter the probe is, the faster is the accessible temporal sampling and the better is the spatial resolution. Furthermore, the more photostable the probe is, the longer is the total accessible duration of an experiment. However, because available bright and photostable probes, e.g. QDs and gold particles are relatively large, SPT experiments at very fast sampling intervals, or for very long durations, have so far mainly only been possible with large probes. But larger probes are typically also more susceptible to artifacts from e.g., steric hindrance as result of membrane topology and molecular crowding, and as a result of probe induced cross-linking due to difficulties in the preparation of large monovalent probes (e.g. gold particles and QDs). Consequently, there are unanswered questions about whether SPT results acquired at very fast sampling intervals are an artifact of the large probe size or are a reflection of the native organization of the plasma membrane.

The primary focus of this review is the relationship between the SPT probe and the SPT results, in particular with respect to the suggested organization of the native plasma membrane. In this review we give a brief introduction to the relevant theoretical expressions and a brief overview of experimental results of motion in a membrane. This is followed by a brief description of SPT and a more detailed description of relevant SPT probes. Finally, we give a summary of recent SPT results with an emphasis on investigations of the plasma membrane organization.

2. MOLECULAR MOTION IN SOLUTION AND IN BIOLOGICAL MEMBRANES

2.1. Theoretical Expressions for Diffusion

A free molecule in a dilute and uniform solution, or in a homogeneous biological membrane, will undergo random Brownian motion that is characterized by a diffusion coefficient D. The diffusion coefficient relates to the thermal energy of the system under study and the frictional drag experienced by the molecule. The distance a molecule diffuses, measured as the mean square displacement (MSD), in a time interval t is linearly dependent on the diffusion coefficient:

$$\mathrm{MSD} = (2\delta)Dt \qquad \text{(Eq. 1)}$$

where δ is the number of dimensions of the system under study. In solution, the molecule is free to diffuse in three dimensions (i.e. δ = 3) while in a membrane the diffusion is within a two dimensional plane (i.e. δ = 2).

The diffusion coefficient, D_S, of a molecule, with a radius of hydration R_H, in solution is given by the Stokes-Einstein equation:

$$D_S = \frac{k_B T}{6\pi\mu_S R_H} \qquad \text{(Eq. 2)}$$

where k_B is the Boltzman constant, T is the absolute temperature, and μ_S is the viscosity of the solution.

Theoretical expressions for the translational diffusion of a molecule embedded within a membrane are much more complex. In the limit where the molecular radii, R, of the membrane molecule is less than or equal to the radii of the lipids, the appropriate theoretical formulations for the translational diffusion, D_M, are given according to the free area theory [13-15]. For membrane molecules with a molecular radii, R, larger than the lipids but where the dimensionless parameter, $\varepsilon = 2\mu_S R / \mu_M h$, is << 1, the translational diffusion, D_M, can be approximated by the hydrodynamic continuum theory which was derived by Saffman and Delbrück [16]:

$$D_M = \frac{k_B T}{6\pi\mu_M h}\left(\ln\left(\frac{\mu_M h}{\mu_S R}\right) - \gamma\right) \qquad \text{(Eq. 3)}$$

In this model, the membrane molecule is approximated as a hard cylinder of radius R and height h, which is embedded within a membrane with viscosity μ_M and surrounded by aqueous phases of viscosity μ_S on both sides, and γ is Euler's constant (γ = 0.5772). This equation has been derived for the case of a homogeneous and continuous lipid bilayer membrane based on the Singer-Nicolson fluid mosaic model [17].

Importantly, the Saffman-Delbrück relation predicts that there is a much weaker dependence on the molecular radii, R, for diffusion in a membrane (∝ ln(1/R)) than in solution (∝ 1/R). Also worth noting is that the lateral diffusion coefficient of molecules that are embedded within a membrane as given by the Saffman-Delbrück equation is much slower than the corresponding diffusion of equally sized molecules in solution as given by the Stokes-Einstein equation. This is because the viscosity in the membrane, μ_M, is about 100 times larger than the viscosity in the surrounding aqueous space, μ_S [16, 18-19]. The large relative ratio of the viscosities further predicts that the diffusion of a molecule within a membrane is determined by the part of the molecule that is embedded within the membrane. This is also the rationale for why an exogenous probe that has been attached to a membrane molecule is expected to only minimally perturb the diffusion, even in cases where the probe is much bigger than the membrane molecule. This is of course only true to a limit as the diffusion coefficient of the probe molecule decreases as its size increases, eventually approaching that of the membrane target molecule. The diffusion coefficients of a membrane species and a probe in solution as given by the Saffman-Delbrück and Stokes-Einstein equations, respectively, are plotted in Fig. (**1**). The plot can be used to estimate the relative influence of an attached probe on the diffusion of a membrane molecule, for example the diffusion coefficient, D_M, for a membrane molecule with R = 1 nm, h = 4 nm, and μ_M/μ_S = 100 is ~4.3 μm^2/sec which corresponds to the diffusion coefficient, D_S, of a molecule in solution with $R_H \approx$ 49 nm. Hence, in this case the probe should be << 49 nm in radius. Worth noting, for the forthcoming discussion, is also that a probe of R_H = 20 nm has a $D_S \approx$ 11 μm^2/sec in water (μ_S = 1.002 cP) at 20 °C.

The Saffman-Delbrück relation (Eq.3) has also been further extended for all values of the dimensionless parameter ε by Hughes et al. [20-22]. In addition a phenomenological model with an inverse dependence of the molecular radii ($1/R$) for membrane molecules in the size range of $0.5 < R < 3$ nm has been recently introduced [23]. None of the alternative models have, however, been conclusively experimentally verified to be better than the Saffman-Delbrück relation in the case of describing the dependence of the molecular radii over a range of $0.5 < R < 7$ nm, and the diffusion coefficient, D_M, for monomers of membrane proteins and small oligomers of membrane spanning peptides and membrane proteins (see also the discussion below) [18-19, 24-25].

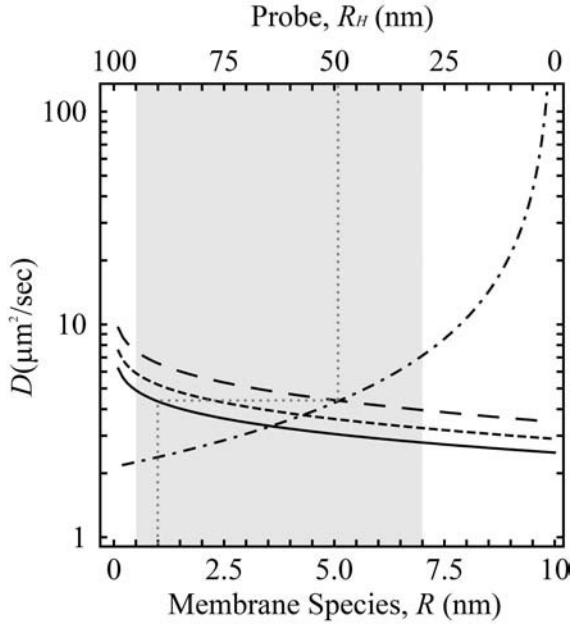

Fig. (1). Theoretical dependences of the diffusion coefficients, D, on the molecular radius, R, for a membrane species embedded within a membrane and on the radius of hydration, R_H, of a probe in solution (dot-dashed line). The dependence for the membrane species was calculated from the Saffman-Delbrück equation with μ_S = 1.002 cP, h = 4 nm, T = 293 K, and for μ_M/μ_S = 100 (solid line), μ_M/μ_S = 80 (short dashed line), μ_M/μ_S = 60 (long dashed line). The dependence for the probe in solution was calculated from the Stokes-Einstein relation with μ_S = 1.002 cP, and T = 293 K. Also shown is the equivalence relation of the diffusion coefficient ($D_M = D_S \approx 4.3$ μm^2/s) of a membrane molecule, with R_H = 1 nm, h = 4 nm, and μ_M/μ_S = 100, and a probe in water with $R_H \approx 49$ nm and μ_S = 1.002 cP at 293 K (grey dotted line). The relevant molecular size range, $0.5 < R < 7$ nm, where the Safmann-Delbrück equation has been validated is shown in gray shading [25].

2.2. Experimental Results for Diffusion in Membranes

In general, for reconstituted lipid membranes, e.g. supported lipid bilayers (SLBs) and giant unilamellar vesicles (GUVs), the translational diffusion rates are typically reported to be in a range of ~1-10 μm^2/sec with variations due to the specific molecules and a number of factors depending on the experimental setup [26]. That is, under otherwise identical conditions, diffusion in SLBs is generally twofold slower than in GUVs, and where measurements in SLBs indicate that there is strong inter-leaflet coupling with identical diffusion coefficients in both leaflets [27]. Furthermore for SLBs, the aqueous layer between the support and the bilayer is important for the motion of molecules [28]. Lipid diffusion has also been found to decrease with increased concentrations of NaCl [29] and hydrogen bonding of lipid head groups, containing mono- and disaccharides, also decreases the diffusion by a factor of as much as three [30]. The diffusion of lipids and proteins in reconstituted membranes are also correlated as an increase of the membrane protein concentration result in slower diffusion of both lipids and proteins [19, 31]. However, the most important factor for the translational diffusion rate in reconstituted model membranes seem to be the lipid composition as the acyl chain length and particularly the presence of sterols (e.g. cholesterol) have large impacts on the diffusion and importantly on the phase of the bilayer under study. In ternary phospholipid-cholesterol-sphingolipid mixtures which are thought to reflect the composition of lipid rafts, micrometer sized liquid-ordered domains rich in cholesterol and sphingolipids form where diffusion rates are 2-20 times slower than in the liquid-disordered phase of the same bilayer [32-33].

The dependency of the molecular radii, R, on the diffusion coefficient, D_M, has been investigated for a large number of systems (e.g. [14, 18-19, 24, 31, 34]). In these studies and others, the existence of two parameter regimes with a transition region for a molecular area of ~1 nm^2 (corresponding to $R \sim 0.6$ nm) has been validated by investigating the diffusion of a combination of lipid and membrane proteins [34-35], and more recently also by systematic investigations of the diffusion of lipid-like macrocyclic polyamides [36] and selectively aggregated membrane spanning peptides [24]. Furthermore, the weak dependency of the diffusion coefficient, D_M, on the molecular radii, R, for larger membrane molecules as predicted by the Saffman-Delbrück relation, has been experimentally validated for e. g. bacteriorhodopsin ($2R = 4.3 \pm 0.5$ nm) in large multilamellar vesicles composed of DMPC [18] and more recently for membrane proteins, ranging in size from $0.5 < R < 4$ nm, which had been incorporated at low protein concentrations (~10-100 proteins/μm^2) in GUVs composed of DOPC: DOPG (3:1, mol:mol) [19]. The relation has further been verified by mesoscopic simulation for $R <$ ~7 nm [25]. Combined, these results suggest that the Saffmann-Delbrück relation (Eq. 3) a reasonable model in the size range of $0.5 < R < 7$ nm (see Fig. (**1**)).

In both the experimental cases, it was also found that the diffusion coefficient of both lipids and proteins depends strongly on the membrane protein density. Peters and Cherry found that the diffusion coefficient of bacteriorhodopsin was reduced from ~3.4 μm^2/sec at a lipid to protein (L/P) ratio of 210:1 (corresponding to ~6,500 proteins/μm^2 with a lipid area of 0.65 nm^2) to ~0.15 μm^2/sec at a more physiologically relevant L/P ratio of 30:1 (corresponding to ~28,000 proteins/μm^2). Ramadurai *et al.* found that the diffusion coefficients of both lipids and proteins decreased linearly with increasing protein concentrations further indicating that molecular crowding plays a significant role in the motion of molecules in membranes. An extrapolation of the linear dependence of the diffusion coefficients to the approximated protein densities of ~25,000 proteins/μm^2 in biological

membranes in this case would result in an order of magnitude decrease in the diffusion coefficient from that observed at protein concentrations of ~3000 proteins/μm^2. This decrease in the diffusion coefficients at greater protein densities is not predicted by the Saffman-Delbrück equation but is consistent with a long known discrepancy between measurements of the thermal motion of lipids and membrane proteins in reconstituted lipid membranes as compared to in the native biological membranes of live cells [37-39].

In contrast to the above results which were obtained in free-standing vesicles, Gambin *et al.*, have investigated the dependence of the molecular radii, R, on the diffusion coefficient, D_M, of single-spanning peptides and multi-pass spanning membrane proteins with a size range of $0.5 < R < 3$ nm in model membranes that are in contact with a solid substrate [23]. Based on these results the authors have introduced a heuristic model with an inverse dependence of the molecular radii ($1/R$) on the diffusion coefficient, D_M, for the tested size range. The validity of these results is, however, likely very strongly influenced by non-specific interactions between the substrate surface and the membrane molecules as is e.g. illustrated by the very slow diffusion that these authors obtained for bacteriorhodopsin (0.08 μm^2/sec) as compared to that measured by Peters and Cherry (3.4 μm^2/sec) in free-standing membranes [18-19].

In contrast, the translational diffusion of lipids and proteins in native biological membranes of live cells is typically found to be at least an order of magnitude slower than in reconstituted membranes, or ~0.01-0.5 μm^2/sec, again with variations due to the specific molecule, cell type, and measurement technique [8, 40]. Ample evidence exist that suggests that the slower diffusion in native membranes is caused by a combination of reasons including molecular crowding, specific molecular interactions, membrane topology, interactions with the actin cytoskeleton, and interactions with nanostructures within the membrane (e.g. caveolae, clathrin coated pits, and hypothesized lipid rafts) [2, 7, 41]. This is perhaps also to be expected considering the complicated composition of the native plasma membrane that is also not an isolated entity but rather contains physical links to both the extracellular space and the cytoplasm that can act as barriers to the translational diffusion of molecules within the lipid bilayer of the membrane. In addition, native membranes are in continuous flux, for example the equivalent of the entire cell surface is estimated to be internalized one to five times per hour [42-43].

3. SINGLE PARTICLE TRACKING

Classical methods like fluorescence recovery after photobleaching (FRAP) and fluorescence correlation spectroscopy (FCS) has found frequent and often successful use in characterizing the lateral dynamics of lipids and proteins in a variety of reconstituted membrane model systems [44]. However, in the case of experiments in native biological membranes, the results from these techniques are more difficult to interpret. For example, FRAP experiments in native biological membranes often result in a fluorescence recovery rate that is not well described by a single diffusing component. In addition, these experiments often also result in only partial fluorescence intensity recovery indicative of the presence of an immobile fraction. Similarly, FCS experiments will often also result in autocorrelation data that is not well described by a single diffusing component [45-46]. While these results suggest that native biological membranes are more complex in organization than reconstituted membrane model systems the full extent of the complexity cannot generally be resolved. In the case of both FRAP and FCS, the resulting experimental data is further an ensemble time average for the fluorescently labeled molecules that diffuse through the observation volume for the duration of the measurement. The heterogeneity behind these averages can only be accessed by using single molecule techniques, with SPT being the technique that allows giving the most information on the individual single molecules [39, 47-49]. SPT is typically done as a 2D measurement although 3D measurements are also possible, however, at a much reduced sampling rate [50].

3.1. Technical Principles of SPT

SPT is a light microscopy technique in which the motion of single molecules, that have been specifically labeled with e.g. a gold particle, a fluorescent dye, protein, or nanoparticle (e.g. QD) are imaged at an acquisition rate of ~10-50,000 Hz [8, 39, 47, 49, 51]. Importantly, using SPT it is possible to greatly surpass the spatial resolution limit of light microscopy, d, which due to the diffraction of light is limited according to the Abbe resolution limit to $d = \lambda/(2NA_{obj})$, where λ is the wavelength of the emitted light, and NA_{obj} is the numerical aperture of the microscope objective. For λ = 500 nm and NA_{obj} = 1.3 the Abbe resolution limit is ~190 nm.

The optical principle behind SPT is that an image of a single point object, acquired from a diffraction limited light microscope, is an Airy pattern, the center of which is the Airy disc and which contains the bulk of the luminous intensity (~84 %). The image of a single molecule can hence for all practical purposes, considering in particular typical signal-to-noise ratios (SNR) of relevant single molecule probes and at appropriate image acquisition settings, be approximated as an Airy disc. The intensity profile of the Airy disc, and hence of a single molecule, is well approximated by a 2D spatial Gaussian, $I \approx I_0 \exp[-r^2/(2w^2)]$, where I_0 is the intensity at the center of the disc, and w is the full width at half maximum (FWHM) intensity and which for fluorescence microscopy is equal to $w \approx 0.61\lambda/NA_{obj}$. The case where the maximum of one Airy disc falls on top of the minimum of another Airy disc is also known as the Rayleigh criterion, and this is the minimum distance by which two single molecules have to be separated in order to still be resolvable as two separate single molecules. In the limit, where the spatial separation of the imaged single molecules are separated by a distance that exceeds the Rayleigh criterion it is possible to determine the centroid position of single molecules very precisely by computational image analysis [47, 49, 52-53]. Using this approach, the localization of single molecules can typically be done with a spatial precision of ~10-40 nm dependent on the SNR, the image acquisition time, and the diffusion rate of the observed molecule.

The thus obtained centroid positions for each single molecule are subsequently linked between image frames in order to be able to obtain trajectories that describe the

motion of each detected single molecule as a function of time. Using these trajectories it is then possible to characterize the motion of the single molecules. This is most typically done by calculating the mean square displacement (MSD), either independently for each detected single molecule trajectory, or in the case where the single molecules trajectories are very short as an average for all detected single molecule trajectories [47, 49, 54]. Using this approach, it is possible to classify the modes of motion by analysis of the shape of the MSD versus time plots. This is most often done as a comparative classification relative to the motion expected for a single molecule that undergoes free Brownian diffusion in a 2D membrane [39, 47, 49]. Alternatively, it is also possible to obtain information about the motion by analysis of the probability distribution of the squared displacements at different time points [47, 55]

A typical result from SPT experiments in plasma membranes is that the MSD plots are timedependent and often show negative curvature, meaning that the diffusion coefficients are greater at shorter distances and time intervals than at longer distances and time intervals [56]. This is indicative of spatial and temporal confinement where the diffusion is free on a spatial and temporal scale much smaller than the characteristic distance between the confining barriers in the membrane. This has resulted in that SPT results are often characterized by a short range diffusion coefficient, D_{micro}, which is determined by the slope from a linear fit of only the first few points (e.g. points 2-4) of the MSD plot, and sometimes also by a long range diffusion coefficient, D_{macro}, which is determined by the slope from a linear fit of a greater number of points on the MSD plot. In the case of a homogenous and continuous membrane such as the case of the fluid lipid mosaic model of Singer and Nicholson [17] the expectation would be that $D_{micro} = D_{macro}$, while in the case of a heterogeneous, compartmentalized membrane the expectation would be that $D_{micro} > D_{macro}$.

3.2. SPT Probes

In SPT there is a very intricate relationship between the optical characteristics of the probe and the accessible sample integration times, the sampling interval, the total duration of an experiment, the spatial resolution, the experimental results, and the interpretation of the results. This is because the brighter the probe is, the faster is the accessible sampling intervals and the better is the spatial resolution, and the more photostable a probe is, the longer is the experimental durations of an experiment.

3.2.1. General Aspects

SPT probes consist of two components, a "specificity module" which renders specificity to a membrane target molecule and a "label module" which renders indirect visibility of the membrane target molecule where relevant membrane target molecules are any molecule that directly interacts with the biological membrane of interest and can e.g. be a lipid, an integral membrane protein, or a lipid-anchored protein. The choice of the combination of the two modules can have a large impact on the execution of an experiment and on the experimental results. The ideal SPT probe would consist of a specificity module with a high specificity towards its membrane target molecule, and a label module which was infinitely bright, to enable experiments at infinite fast time intervals, and infinitely stable, to enable experiments for an infinite time period. The probe, as well as the specificity module, should ideally be monovalent to prevent probe induced cross-linking, which could result in the activation of signaling pathways or reduced mobility [39]. The probe size, which as discussed could be much larger than the target membrane molecule without perturbing the observed diffusion coefficient, should yet preferably be minimal in size in order to maximize access to the membrane target molecule and to minimize possible steric hindrance. Steric hindrance could for example result in that only a subset of target molecules is accessible for labeling e.g. due to molecular crowding or membrane topology [41].

Commonly used SPT probes consist of a combination of labels like; fluorescent dyes, FPs, and QDs, and gold particles, and specificity modules like; antibodies (Abs), Fab fragments, and sAv *etc*. The probes and the individual parts are shown according to their relative sizes in Fig. (**2A**). In Fig. (**2B**), experimental FCS autocorrelation curves of probe molecule diffusing in solution are shown together with that for the diffusion of DPPE-Rhodamine in a GUV. The corresponding diffusion coefficients and hydrodynamic radii are given in Table **1**. The last column in this table gives the ratio between the probe diffusion in solution and the diffusion of a labeled membrane target molecule (DPPE-Rhodamine) in a GUV, as an indicator for the frictional drag effect of the probe size on diffusion of a membrane target molecule, see also to the discussion in relation to Fig. (**1**). This ratio should preferable be >>1 for the probe to have minimal influence on the motion of the membrane target molecule. Properties of specificity modules and labels are further discussed below.

3.2.2. Specificity Modules

The specificity modules used in SPT can generally be classified into two categories; those that have affinities for naturally occurring membrane targets e.g. Abs, DNA and RNA aptamers, lectins, and various toxins such as cholera toxin subunit B (CTB), and those that first need the insertion of an artificial peptide or protein epitope tag in the target molecule in order to introduce labeling specificity [58-59]. Epitope tags are often introduced via genetic insertions of sequences e.g. the biotin ligase acceptor peptide (BLAP) for streptavidin, [60], the acyl carrier protein (ACP) for Coenzyme A (CoA) derivatives [61], the SNAP tag for benzylguanine derivatives [62], and tetra-cysteine peptide motifs for the biarsenical derivatives FlAsH and ReAsH [63]. A special case is the FPs since the tag and the specificity is combined in one unit together with the visible label module genetically expressed in immediate continuation of the target protein giving a pseudo-intrinsic probe with absolute specificity. In addition to the artifacts that a modification can induce, the main disadvantage of genetically introduced tags is that the modified proteins are typically expressed at non-physiological levels [64].

The size of the specificity module can change the total size of the entire probe considerably. This is especially the case when labeling is done by immunolabeling using both a primary and secondary Ab, sometimes even in combination

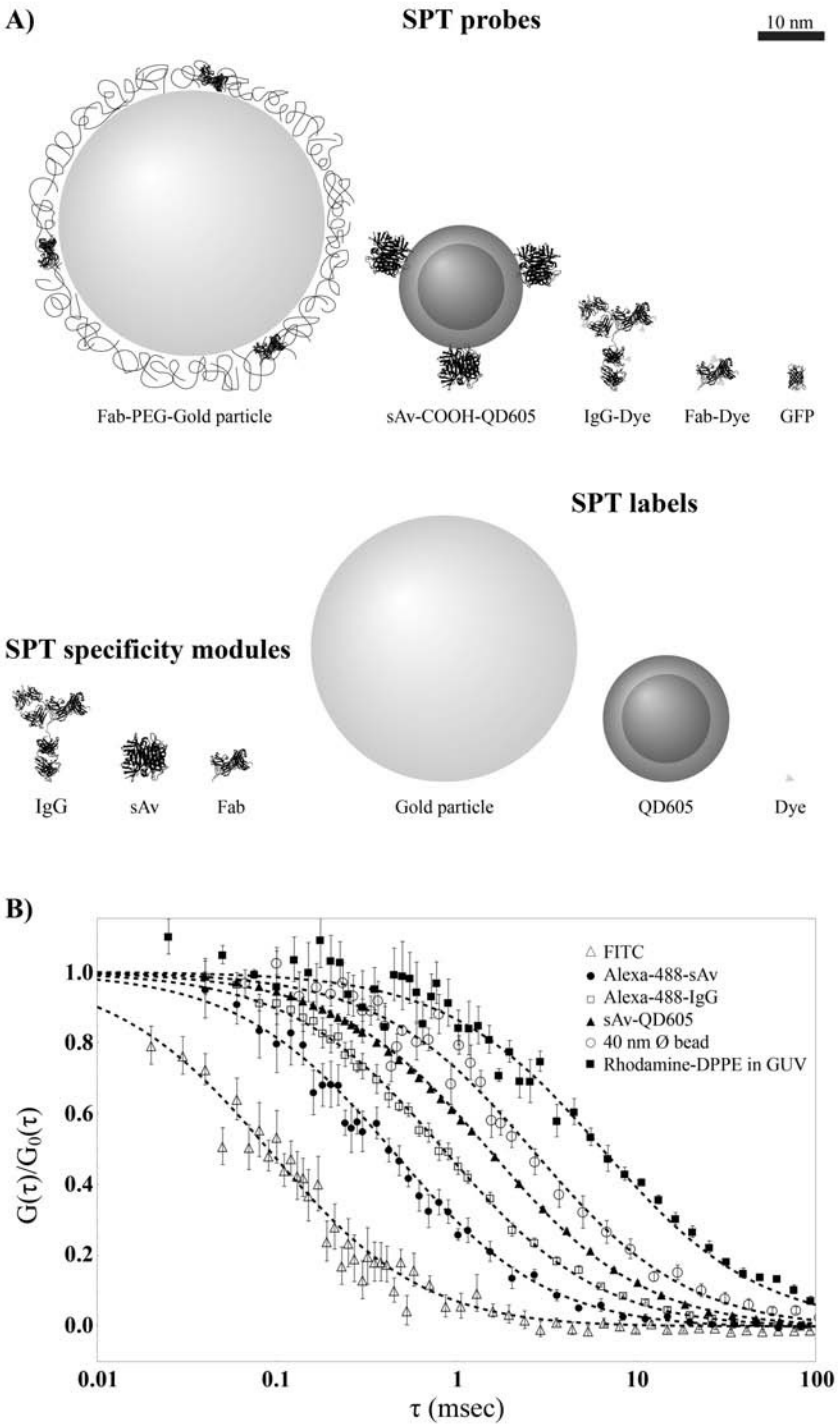

Fig. (2). A) Common probes used in SPT and their individual modules represented illustrating their relative sizes as measured by FCS. The probes are: Ø 40 nm (Fab-PEG-) gold particle coated with a PEG polymer and functionalized with Fab fragments ($R_H \gtrsim 25$ nm), sAv-functionalized COOH-QDs emitting at 605 nm (sAv-COOH-QD605, $R_H \approx 9.7$ nm), dye labeled immunoglobulin G (IgG-dye, $R_H \approx 5.8$ nm), dye labeled Fab fragment (Fab-dye, $R_H \approx 2.9$ nm [123]), and the green fluorescent protein (GFP, $R_H \approx 2.3$ nm [57]). The shown specificity modules are: IgG, Fab and streptavidin (sAv, $R_H \approx 3.4$ nm), whereas the un-functionalized labels are: Ø 40 nm gold particle, COOH-QD605 ($R_H \approx 6.0$ nm), and a FITC dye ($R_H \approx 0.7$ nm). **B**) FCS correlation curves for typical SPT probes in solution compared to that of Rhodamine-DPPE in a lipid GUV. The raw data shown is for the mean±s.e.m normalized correlation function from n = 5 or 6 independent correlation curves. The FCS data for the probes in solution was curve fit to $G(\tau) = G_0(\tau)\ (1+8D_S\tau/r^2)^{-1}(1+8D_S\tau/z^2)^{-1/2}$ (solid lines) while the FCS data for lipid diffusion in a GUV was fit to $G(\tau) = G_0(\tau)\ (1+8D_M\tau/r^2)^{-1}$ (dashed line). The values for the diffusion coefficient obtained from the curve fit are given in Table **1**.

Table 1. Diffusion coefficients, D_S, and hydrodynamic radii, R_h, of SPT probe molecules in solution obtained by FCS. The diffusion coefficient of rhodamine-DPPE in a GUV was D_M = 4.5±0.3 μm²/sec. This value is used in the ratio D_S/D_M to estimate the diffusion effect of the probe size relative to the membrane target. A value >>1 means that the probe has minimal effect.

Probe	R_h (nm) mean±s.e.m.	D_S (μm²/sec) mean±s.e.m.	D_S/D_M mean±s.e.m.
Ø 40 nm bead	20.3±3.0	10.7±1.6	2.4±0.4
sAv-QD605	9.7±0.5	21.3±1.2	4.7±0.4
Alexa488- IgG	5.8±0.2	36.5±1.6	8.1±0.6
Alexa488-sAv	3.4±0.2	64.0±3.9	14±1.3
GFP [57]	2.3±0.05	93.2±2.2	21±1.5
FITC	0.7±0.2	316±72	70±17

with labeled sAv. In addition, some specificity modules are multivalent, e.g. Abs which are bivalent, native sAv which is tetravalent, and CTB which is pentavalent, and are hence capable of inducing cross-linking of the membrane target molecules. The problem of cross-linking can be circumvented by use of monovalent Fab Ab fragments or genetically engineered monovalent streptavidin [65]. Probe multivalency is also a problem in the case where the labels are gold particles or QDs. This is because these labels contain multiple surface binding sites for the specificity modules and because as a result any reaction between the two is limited by Poisson statistics. Hence even reaction conditions that strongly favor no binding of the specificity module to the label will result in a population of multivalent labels, e.g. a 2:1 (mol:mol) ratio of label to specificity module which, assuming a 100 % reaction yield, would result in ~60 % of labels with no specificity module, ~30 % of labels with one specificity module, ~8 % of labels with two specificity modules, and ~2 % of labels with more than 2 specificity modules. The preparation of monovalent probes, in the case where the label is a particle, thus requires a purification step capable of separating those particles that have only one specificity module from the rest. This has been accomplished by agarose gel electrophoresis of QDs that had been reacted with sAv [66-68] or poly-ethylene glycol (PEG) polymers [69], and for gold particles that had been reacted with DNA [70].

3.2.3. Labels

3.2.3.1. Fluorescent Dyes and Fluorescent Proteins

The smallest possible SPT labels are small organic fluorescent dyes. These can e.g. be directly attached to lipids creating fluorescent lipid analogs (e.g. Rhodamine-DPPE, NBD-DPPC, Bodipy-Cholesterol *etc.*). However, fluorescent lipid analogs, which may either have been modified in the hydrophobic acyl chain tails or the hydrophilic head groups, have significantly different chemical structure than the corresponding unmodified lipids and as a consequence the behavior of fluorescent lipids will often be altered. This is especially true for cholesterol, since attached dyes are almost equal in size to cholesterol, are often polar or even charged. Consequently no existing fluorescent cholesterol analog mimics the properties of native cholesterol [71]. Specific protein labeling with small dyes is also possible with for example systems like FlAsH, ReAsH, BLAP, ACP, SNAP and CLIP systems [59, 72], were the dyes can bind directly to peptide tags in the target protein and render a probe that is smaller or comparable in size to FPs. However, in most cases fluorescent dyes are used in combination with e.g. intact Abs, Ab Fab fragments, or sAv in order to confer specificity towards the molecular target, hence increasing the size of the label and with the potential risk of causing cross-linking artifacts as discussed above.

The main disadvantages of fluorescent dyes are low brightness and poor photo-stability, thereby preventing single molecule imaging at very fast time intervals (not bright enough) and for long time durations (not stable enough). However, recently developed dyes like e.g. Alexa-647, which has a high molar extinction coefficient (ε = 220,000 $M^{-1}cm^{-1}$ at 647 nm), moderate quantum yield (QY = 0.33), and a high saturation intensity, has enabled SPT imaging at image acquisition rates up to 2000 Hz, but only for less than ten images [73]. In contrast, SPT experiments with the dye Atto647N (ε = 150,000 $M^{-1}cm^{-1}$ at 644 nm, QY = 0.65) have been reported at 10 Hz, but with a mean time duration of single molecule trajectories of 15 seconds [74]. FPs, like fluorescent dyes, also exist in a wide range of different colors [75], and in a variety of modified forms such as e.g. photo-switchable FPs. The optical properties of FPs in terms of brightness and stability, however, are inferior to that of the better dyes, e.g. enhanced green fluorescent protein has a molar extinction coefficient, ε = 56,000 $M^{-1}cm^{-1}$ at 484 nm, and a QY of 0.6. As a result, SPT with FPs is typically performed at 10-30 Hz, but has in the case of enhanced yellow FP (EYFP) been accomplished even at 200 Hz [76]. In both cases, the duration is typically limited to less than twenty image frames before the FPs irreversibly photobleach.

3.2.3.2. Quantum Dots

QDs are semi-conductor nanoparticles that are composed of inorganic cores of ~Ø 2-10 nm and which are the origin for their fluorescence properties with the size relating to the emission color. However, stabilization and functionalization of QDs in aqueous media requires that additional layers are added resulting in a final total size of ~Ø 15-30 nm. Functionalization of QDs with e.g. sAv [60], CoA [77], CTB

[78], Fab fragments [79], or any other preferred bio-molecule is relatively standardized and easy, but the number of attached bio-molecules, and hence the valence of the entire QD is difficult to control, with potential risk of cross-linking target molecules when used in SPT. The size of some QDs was also shown to limit their access to synapses [80], but monovalent and size-reduced QDs have been made with markedly improved accessibility [67-68]. More improvements along this direction are also expected.

The fluorescent properties of QDs are far superior to those of dyes and FPs. They have very high extinction coefficients (ε = 1,100,000 $M^{-1}cm^{-1}$ for sAv-QD605 at 488 nm) and yet moderate quantum yields (QY ≈ 0.5) which account for their extreme brightness. In our laboratory we have successfully imaged single moving QDs on the cell surface at rates up to 1760 Hz and ~0.5 msec integration time with the limiting factor being the readout speed of the camera. In terms of stability, the QDs do not photobleach easily on a time scale relevant for most SPT studies, thus they can be readily imaged for periods of several tens of seconds to minutes. A limitation to this being the observed blinking (alternation between a fluorescent on- and an off-state) [81] when imaged at the single molecule level, making SPT linking algorithms more demanding [52-53]. QDs of different colors show similar and broad excitation, and have narrow symmetric emission spectra, making them ideal for multi-color imaging. This advantage has also been used in demonstrating that multispecies SPT with QDs is possible [66, 82]. More detailed information on QDs is available from other sources [83-86].

3.2.3.3. Gold Particles

Colloidal gold particles differ from the other labels in that the detected signal is based on light scattering rather than fluorescence, where the amount of scattered light is strongly dependent on the particle size. The scattering nature of the gold particles means that SPT with gold particles can only be performed for a single type of molecule at a time. In the case of SPT on native plasma membranes, the SNR typically dictates that Ø 40 nm non-functionalized gold particles are required. The large size of gold particles used in SPT is likely to restrict access to certain areas on the cell surface due to steric effects. Furthermore, as shown in Table **1**, the diffusion of a Ø 40 nm particle in solution is only twice that of a lipid molecule diffusing in a model membrane, thus gold particles are likely to have a notable influence on the diffusion of the membrane target molecules.

Specificity of gold particles is accomplished by charge mediated absorption of relevant specificity modules such as Abs or Fab fragments to the surface of the particles [87]. Similarly to QDs, however, colloidal gold particles also have to be stabilized for use in physiological conditions, in this case in order to prevent aggregation in presence of salts. Stabilization is typically accomplished by absorption of proteins to also include the mixed absorption of relevant specificity modules in combination with passive ligands that can be proteins e.g. Abs or Fab fragments that have no binding specificity at the investigated membrane, BSA (R_H ≈ 3 nm) or poly-ethylene glycol (PEG) polymers e.g. Carbowax 20M which has an average molecular weight of 17.5 kDa [88] and an estimated radius of gyration, $R_g \approx 9$ nm (using $R_g \approx N_0^{3/4}$, where N_0 is the number of PEG monomers). The functionalization and stabilization of gold particles will thus most likely add at least ~10 nm to the diameter. Functionalized gold particles are hence ~2 times larger in diameter than a QD, and correspondingly have an 8 times larger volume. However, in terms of signal, gold particles are beyond comparison to any of the other labels. Accordingly, Kusumi and co-workers have performed SPT with gold particles at a frame rate of 50,000 Hz over extended time periods [89].

3.3. SPT Results

SPT has been in particular instrumental in revealing the extent of the spatio-temporal heterogeneity in the organization of plasma membranes [52, 73, 87, 90-92]. This is because SPT is currently the experimental method that offers the best available combination in spatial and temporal resolution. This has enabled SPT to detect very small (~20-50 nm) and transient (~1-10 msec) organization as well as small (~100-300 nm) and longer lived (~1 sec) organization within the mammalian plasma membrane [87, 90, 93-94]. In general, the SPT results of the detected modes of motion of lipids and membrane proteins in the plasma membrane are, independent of the SPT probe (and associated sampling intervals and the time durations) very heterogeneous, typically always displaying a large range of modes of motion to include free diffusion, confined diffusion, and combinations thereof [54, 74, 87, 92, 95]. A schematic of some typical modes of motion is found in Fig. (**3**).

A frequent use of SPT is investigations of the plasma membrane nanostructure to include interactions with e.g. caveolae, clathrin coated pits, and hypothesized lipid rafts [54, 73-74, 82, 87, 89-93, 96-101]. In these studies, SPT sampling intervals have ranged from an extreme speed at 50,000 Hz with Ø 40 nm gold particles [89, 93], 1000-1760 Hz with QDs [95], 1000-2000 Hz with Alexa-647 [73], 200 Hz with EYFP [99], to a more typical sampling of ~30 Hz or slower for all the different labels. SPT data has furthermore been collected for a variety of time durations ranging from many tens of thousands of images for Ø 40 nm gold particles, thousands to a few tens of thousands of images for QDs, to less than ten to a few hundreds of images for fluorescent dyes and FPs. In a comparison of this SPT data it is apparent that the results of plasma membrane nanostructure are dependent on the acquisition parameters and consequently possibly also on the SPT probes.

Experiments at very fast temporal sampling rates of 40-50 kHz have so far only been possible in the Kusumi lab and by using Ø 40 nm gold particles as the label [2, 87, 89, 93, 101]. A unifying result from these studies is that all possible types of membrane target molecules, e.g. lipids, lipid anchored membrane proteins, and single and multi-pass integral membrane proteins, are confined in compartment sizes of ~30-250 nm for average residency times of ~1-20 msec, where the characteristic sizes and times were found to vary in a cell dependent fashion [2, 100]. This confinement, which has been coined hop-diffusion, is dependent on the actin cytoskeleton, but neither on the presence of cholesterol nor on the removal of the major fraction of the extracellular domains of membrane protein or the extracellular matrix [2, 87, 100].

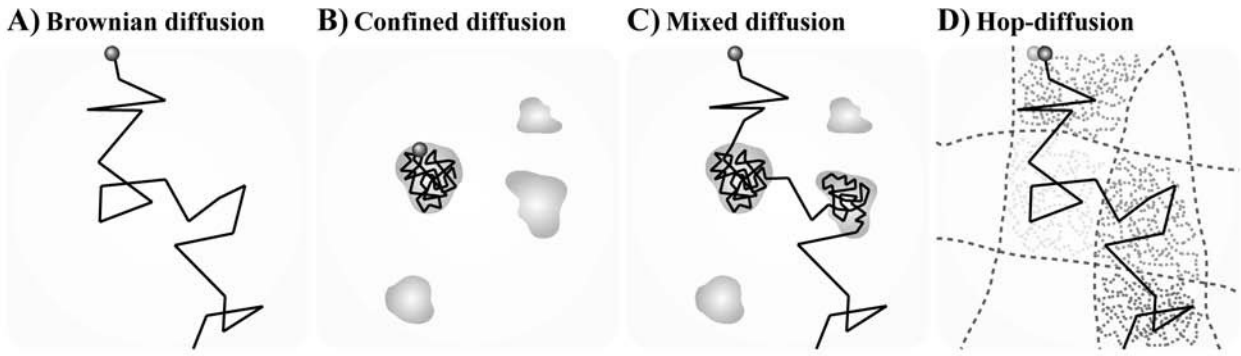

Fig. (3). Sketch of various diffusive behaviors in a membrane dependent on the dominating underlying structure. **A**) Brownian diffusion; the molecule is not influenced by any membrane structures. **B**) Confined diffusion where the motion is limited to a restricted area (dark grey) of the membrane. **C**) Mixed diffusion with areas of free diffusion and areas of confined diffusion (anomalous sub-diffusion). **D**) Hop-diffusion where the molecule is temporarily confined (dotted grey trajectory) by the underlying cytoskeleton (dashed lines). This phenomenon is only observed for SPT with large probes when imaging at very fast imaging rate, whereas at slow imaging rates the diffusion will appear free (black trajectory).

In the case of one cell line, NRK fibroblasts, the mean short range diffusion coefficient, D_{micro}, over a 100 μs time window, of the lipid DOPE within these compartments (~230 nm) has been reported to be 5.4 μm^2/sec [87], with similar numbers also being reported in the same cell type for an integral membrane protein, the transferrin receptor (D_{micro} = 5.2 μm^2/sec) [87], and a 7-transmembrane protein, the G-coupled protein receptor (GPCR) μ-opiod receptor (D_{micro} = 4.2 μm^2/sec) [93]. The mean long range diffusion coefficient, D_{macro}, over a 100 ms time window in these studies and for these molecules were typically independent of the label type (gold particles or Cy3) in the range of ~0.1-0.5 μm^2/sec [87, 93, 100].

These results are particular surprising because even the phospholipids DOPE, and GPI-anchored proteins, neither of which have direct contact with the cytoplasmic space, are confined in compartments equal in size to those found for integral membrane proteins such as the transferrin receptor and the GPCR receptor [87, 89, 93, 100-101]. In response to these results, the anchored protein picket model has been proposed. In this model, membrane proteins that are anchored to and aligned with the actin cytoskeleton act as pickets in a fence to restrict the free lateral diffusion of molecules in the membrane by a combination of steric hindrance and hydrodynamic friction [2, 8]. Because many of the membrane proteins extend into the extracellular space this model could then explain why membrane target molecules such as lipids and lipid anchored proteins also undergo hop-diffusion. This model is further supported by electron microscopy data that shows that actin filaments are in close proximity of the plasma membrane and forms compartments that are similar in size to those conferred by the SPT data [102].

Another surprising aspect of this work is the proposed magnitudes of the diffusion coefficients of lipids and proteins alike within the confinement zones of ~5-8 μm^2/sec [87, 89, 93, 100]. This is equal in magnitude to that found in reconstituted model membranes, but only at much lower proteins densities than are considered to be physiologically relevant [18-19]. The authors further justifies the proposed magnitude of the diffusion coefficient by reporting that similar magnitudes are also measured in cell blebs that are absent of actin cytoskeleton. However, the protocol used for preparing the blebs (incubation with 1 mM menadione for 1 h at 37 ^oC) has also been shown to reduce the cell surface density of transferrin and LDL receptor by ~70 % by inhibition of receptor recycling after incubation with only one fifth the dose of menadione (200 μM) under similar conditions [103]. Similarly, reduction of the total protein content has further been demonstrated for other bleb forming protocols [104]. The reported short range diffusion coefficients in NRK cells for DOPE (D_{micro} = 5.4 μm^2/sec), transferrin (D_{micro} = 5.2 μm^2/sec), and μ-opiod receptor (D_{micro} = 4.2 μm^2/sec) also suggests that the dependence on the diffusion coefficient on the molecular radii within the confinement zones is weaker even than that suggested by the Saffman-Delbrück equation. We also note that the reported magnitude of the diffusion coefficients of the lipids and protein within the confinement zones are equal to, or at best only one half the expected magnitude of, the diffusion coefficient of the free gold particles in solution hence suggesting that there should also be a significant frictional drag effect of the probe on the measured diffusion coefficient of the membrane target molecules (see also Fig. (**1**)).

A caveat in these studies is of course that these results are so far obtained with one technique, SPT with Ø 40 nm gold particles. In response to this, Wieser *et al.* used SPT with significantly smaller probes consisting of either a Fab fragment ($R_H \approx$ 2.9 nm) or an intact Ab labeled with the fluorescent dye Alexa-647 ($R_H \approx$ 5.8 nm) in order to investigate the high-speed motion of the GPI-anchored protein CD59 in T24 (ECV) cells [73]. In this cell line, Murase *et al.* had previously reported that the lipid DOPE undergoes hop diffusion between compartments with a mean (±s.d.) size of 120±53 nm for an average residency time of 16 msec and with a *D* of 0.20±0.08 μm^2/sec (for gold-labeled DOPE with a 100 msec time window) [100]. In these experiments, SPT data was collected with acquisition times ranging from 50 μsec to 1 msec and with sampling intervals ranging from ~10-2000 Hz. The representative duration in the case of using Fab fragments at 1000 Hz was only six image frames hence prohibiting individual trajectory analysis. Consequently all data

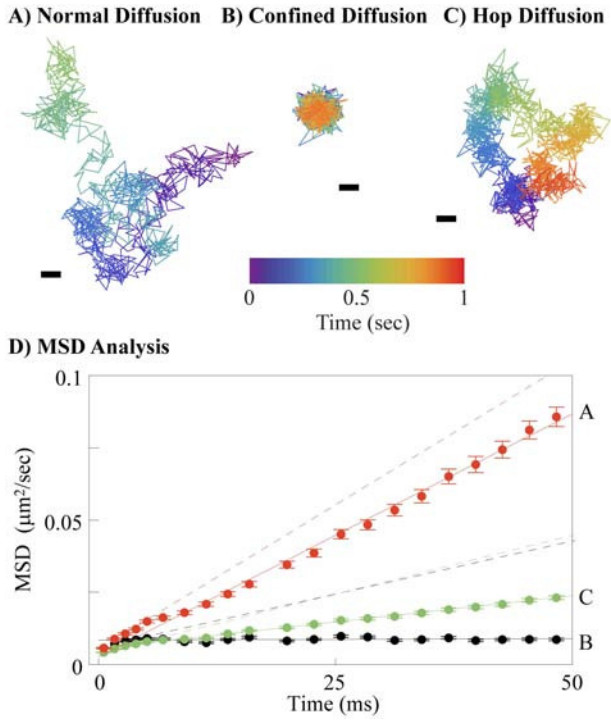

Fig. (4). Single QD trajectories showing the diffusion of a lipid, biotin-cap-DPPE, which had been artificially bulk loaded into a mouse embryo fibroblast and labeled with sAv-QD655. Images were acquired with 0.52 msec integration at 1760 Hz and analyzed by standard particle tracking methods. The points in each trajectory are linearly color coded as a function of the time after the start of the first point in the respective trajectory. In these experiments, we always see three types of motion indicative of the heterogeneous nature of the plasma membrane, **A**) approximately normal diffusion (total trajectory time ~930 pts corresponding to ~0.53 sec), **B**) very confined diffusion (total trajectory time ~1550 pts corresponding to ~0.88 sec), **C**) and hop diffusion (total trajectory time ~1670 pts, 0.95 sec). The mode of motion of each trajectory was further analyzed by calculating the mean squared displacement (MSD) of each trajectory separately as a function of time, t and by subsequent curve fitting to MSD = $4D_{micro/macro}t$ for two separate time windows, 1) short term diffusion, D_{micro}, corresponding to analysis of image frame 2-4 (δt ~1.5 msec), and 2) long term diffusion, D_{macro}, corresponding to analysis of image frames 2-88 (δt ~50 msec). The results of this analysis was for A) normal diffusion (red points) D_{micro} ≈ 0.50 μm^2/sec (best fit, red dashed line), D_{macro} ≈ 0.42 μm^2/sec (best fit, red line), B) very confined (immobile) diffusion (black points) D_{micro} ≈ 0.20 μm^2/sec (best fit, black dashed line), D_{macro} ≈ 0.00 μm^2/sec (best fit, black line), and C) hop diffusion (green points) D_{micro} ≈ 0.20 μm^2/sec (best fit, green dashed line) D_{macro} ≈ 0.09 μm^2/sec (best fit, green line). Scale bar 100 nm.

analysis was done by time averaging over multiple trajectories from several cells but by using both MSD analysis and by analysis of the probability distributions of the squared displacements. The conclusions from this analysis was that the lipid anchored protein CD59, on average, undergoes normal Brownian diffusion ($D_{micro} = D_{macro}$) for all conditions that were tested. The diffusion coefficients at 37 °C were found to range from 0.46±0.05 μm^2/sec for Fab fragments acquired at ~1000 Hz to 0.17±0.01 μm^2/sec with intact Abs acquired at ~600 Hz, thus indicating that in this case there is a very strong dependence on the probe, from a combination of probe induced cross-linking and possibly also probe size. This data hence indicates that the hop-diffusion that is observed by use of gold particles may very well be an artifact of the probe. However, this data while acquired with a much less invasive probe is yet limited by that the representative trajectory duration (~6 msec) is much less than the reported lifetime (~16 msec) of the proposed domains. Hence, we believe that further work is required to validate or disprove the concept of hop diffusion as it is currently presented.

Along this line, we have also initiated work in order to be able to validate the presented concept of hop-diffusion. In our preliminary results, we have imaged the molecular motion of an artificial lipid, biotin-cap-DPPE, in mouse embryo fibroblasts (MEFs) by using commercially available sAv-QDs emitting at 655 nm (R_H ≈ 11.4 nm; data not shown) in combination with an EMCCD camera (DU-860; Andor). In these experiments we have used an illumination time of ~0.52 msec and a sampling rate of ~1760 Hz Fig. (**4**). A preliminary analysis of this data indicates that the motion of a majority of lipids is restricted at short time intervals (~50-200 msec) to domains with a size range of ~100-200 nm in diameter and with a D_{micro} (time window of ~1.5 msec, points 2-4) of 0.20 μm^2/sec and a D_{macro} (time window of ~50 msec, points 2-88) of 0.09 μm^2/sec. This data suggests that lipids that have been labeled with sAv-QDs in MEFs behave in a similar fashion to lipids that have been labeled with larger gold particles [87, 100]. However, much further statistical analysis of this data is needed to fully characterize the observed confinement in this case. This data is however of course also subject to all the limitations associated with the use of larger probes.

SPT acquired at ~10-30 Hz reveals an entirely different picture for the plasma membrane organization. At this slower sampling rate hop diffusion is not observed. Instead observed confinement regions are either larger, longer lived or both. For example, SPT data acquired at ~30 Hz has identified membrane areas of ~100-300 nm diameter in which certain membrane targeting molecules (e.g. GPI-anchored proteins, GSLs, and phospholipids) are temporally confined to, but free to move within, for several seconds [54, 90, 94, 96, 105]. These areas, which are sometimes referred to as transient confinement zones (TCZs), are identified by probabilistic means by comparison of the instantaneous displacements in comparison to the expected displacements for a molecule that undergoes random diffusion [94, 105]. TCZs have been shown to be cholesterol dependent and to be dependent on GSL synthesis. This has led to the suggestion that TCZs are a kind of lipid raft [96, 105]. However, the size and lifetimes of identified TCZs are dependent on the time resolution of SPT [105]. Furthermore, it has been reported that TCZs are not observed even in data acquired at 30 Hz in the absence of probe-induced cross-linking [106]. This suggests that TCZs are an experimental artifact that is induced by probe induced cross-linking. SPT has also been used in this context to investigate sparse signaling of membrane proteins by use of intentionally multivalent gold particles. Using this method Chen *et al.* have found that GPI-anchored proteins undergo transient anchorage for periods ranging from 300 msec to 10

sec [92]. This transient anchorage was found to be dependent on cholesterol and Src family kinases [92]. Using a similar method, Suzuki *et al.* have also shown that small clusters of CD59 will transiently recruit several intracellular signaling molecules resulting in what the authors have termed stimulation-induced temporary arrest of lateral diffusion (STALL) with an average duration of 0.57 sec occurring every 2 sec [91, 101].

In addition to the proposed nanostructures observed by SPT, SPT has also been used to identify specific interactions between plasma membrane molecules and molecular protein targets and the actin cytoskeleton inside the cell [52, 82, 107-113].

4. COMPLEMENTARY TECHNIQUES

Many other forms of traditional light microscopy techniques, for example FRAP and FCS have the sufficient temporal resolution to be able to resolve transient structures, down to within a lifetime range of milliseconds to seconds, but the spatial resolution of information from the bleach spot and focal spot, respectively, are limited by diffraction to >200 nm (for reviews of traditional light microscopy techniques used to study membrane lateral organization see [40, 44]). In contrast, electron microscopy, which has sufficient spatial resolution but of course no temporal resolution and which has been used to visualize relatively static nanostructures such as caveolae and clathrin-coated pits, has so far not been able to conclusively resolve additional nanostructure in the plasma membrane. More recently, new light microscopy techniques have also been introduced which offer sub-diffraction limited spatial resolution, for example the related techniques photoactivated localization microscopy (PALM) and stochastic reconstruction microscopy (STORM). These methods can reach a spatial resolution of 20-40 nm by computational fitting of single molecule point spread functions in an image series where only a subset of labels are emitting in each frame [114-115], but the best temporal resolution reached by these techniques is 50 msec in the so-called sptPALM [116]. Perhaps the most significant developments, however, has been the introduction of stimulated emission depletion FCS (STED-FCS) by Eggeling *et al.* where the focal spot of FCS is significantly decreased to ~30 nm [117], and an orthogonal confocal microscope based tracking technique developed by the same group reaching the same spatial and temporal resolution by determining the positions of dye labeled molecules using three point detectors placed in close proximity [118]. By these techniques it has been shown that sphingolipids in contrast to phospholipids are temporarily trapped for ~10 msec in ~10-20 nm sized domains in a cholesterol dependent manner [117-118].

5. OUTLOOK AND CONCLUSION

Gaining a better understanding of the molecular organization of the mammalian plasma membrane is expected to have far reaching consequences and may offer many rewards in biomedicine. For example, possible spatial regulation of cell signaling as a result of plasma membrane organization could help explain how specificity in externally mediated cell signaling cascades is maintained in the cytoplasm [119]. This is especially relevant considering that intracellular cell signaling cascades are extremely complex and involve multiple overlapping signaling second messengers, e.g. phosphoinositides (PtdIns) such as PtdIns(3,4,5)P_3 and PtdIns(4,5)P_2 which are downstream mediators in a variety of cell signaling pathways that are activated by an equally diverse number of extracellular stimuli including growth factor receptors, GPCRs, and immunoglobulin super family receptors [120]. Spatial regulation in cell signaling also offers the potential for drug targeting to receptor complexes rather than single receptors, a mechanism that could increase drug specificity and avidity.

A general consensus in the field is that the organization of the native plasma membrane is very heterogeneous and complex. This consensus view is strongly supported by SPT results which show a range of molecular motions (e.g. Brownian, confined and combinations thereof) and nanostructures from very transient (<100 msec) and small (<100 nm) to more stable (>1 sec) and large (>100 nm). A consequence of the observed heterogeneity is also that the lateral motion in the plasma membrane is time dependent such that the detection of structures requires that the accessible temporal sampling is faster, the duration is longer, and the spatial resolution is less than the lifetime and size of the structures. A second consequence is that the SPT results are strongly influenced by the probes that are used since it is the optical properties of the probe that dictates the accessible experimental spatial and temporal resolution. This is especially apparent in the case of hop diffusion which has repeatedly been shown by use of SPT with large functionalized gold particles (of ~Ø50 nm), since the required very fast sampling intervals, and for long durations, have thus far only been possible with these large probes. However, there are still many open questions about whether the results with larger probes in this case are a reflection of the membrane organization or is an artifact stemming from the probe size (e.g. frictional drag, steric interactions, and artificially induced cross-linking), in particular with respect to the reported magnitude of the diffusion coefficient. In contrast, even though SPT experiments with fluorescent dyes and proteins are less invasive, the temporal sampling is either too slow or the duration is too short to directly and conclusively observe or rule out transient and small structures such as those suggested for hop diffusion. The appropriate choice of probe in an SPT experiment should then always be made in relation to the relevant temporal scales, both in terms of the frequency and the duration, of the phenomena that are under investigation. Furthermore, considering the intricate link that exists in SPT between the probe and the results as well as the potential risks of probe induced artifacts, it is of utmost importance that all SPT results are carefully cross-validated, either with SPT using different probes, or alternative by the emerging techniques that are in some cases enabling investigations at equivalent spatial and temporal resolutions.

In relation to one of the other suggested nanostructures in the plasma membrane, the lipid rafts, there are also many remaining questions. In model membranes, lipid mixtures that are thought to be representative of lipid rafts form micrometer sized domains [33]. These domains are not observed in live cells, even though their formation can be artificially induced in cell blebs and plasma membrane spheres (PMS) [121-122]. Membrane blebs and PMS have in com-

mon that they exclude links to the actin cytoskeleton. A plausible explanation is then that actin filaments, in addition to restricting the free motion of membrane species as suggested by SPT results with gold particles, also are a limiting factor in the formation of large lipid domains, and which as a consequence only exist as small domains [117-118]. This possibility has previously been suggested by Kusumi *et al.* [2]. Membrane topology, which is caused by e.g. actin cytoskeleton extensions and membrane ruffling could also have a significant influence on the observed molecular motion in the plasma membrane and should not be forgotten in the discussion of plasma membrane lateral organization [41].

ACKNOWLEDGEMENTS

We thank Jakub Kubiak for the FCS data of rhodamine-DPPE in GUVs and Thomas E. Rasmussen for the FCS data of FITC, sAv, IgG, and Ø 40 nm beads. This work was supported by grants from the Danish National Research Foundation (to MEMPHYS), the Villum Kann Rasmussen Foundation (to BioNET), the Lundbeck Foundation (to B. C. L), the Novo Nordisk Foundation (to B. C. L.), the Leo Pharma Research Foundation (to B. C. L.). This work furthermore benefitted from the establishment of the Danish Biomedical Imaging Center (DaMBIC) at the University of Southern Denmark by Danish Ministry of Science.

ABBREVIATIONS

Ab	=	Antibody
ACP	=	Acyl carrier protein
BLAP	=	Biotin ligase acceptor peptide
CoA	=	Coenzyme A
CTB	=	Cholera toxin subunit B
D	=	Diffusion coefficient
D_M	=	Diffusion coefficient in membrane
D_{macro}	=	Long range diffusion coefficient
D_{micro}	=	Short range diffusion coefficient
D_S	=	Diffusion coefficient in solution
ε	=	Molar extinction coefficient
FCS	=	Fluorescence correlation spectroscopy
FP	=	Fluorescent protein
FRAP	=	Fluorescence recovery after photobleaching
FWHM	=	Full width at half maximum
GSL	=	Glycosphingolipid
GUV	=	Giant unilamellar vesicle
IgG	=	Immunoglobulin G
μ_M	=	Membrane viscosity
μ_S	=	Solution viscosity
MSD	=	Mean square displacement
PALM	=	Photoactivated localization microscopy
QD	=	Quantum dot
QY	=	Quantum yield
R	=	Molecular radii
R_H	=	Radius of hydration
sAv	=	Streptavidin
SLB	=	Supported lipid bilayer
SMFT	=	Single molecule fluorescence tracking
SNR	=	Signal to noise ratio
SPT	=	Single particle tracking
STED	=	Stimulated emission depletion
STORM	=	Stochastic reconstruction microscopy
Ø	=	Diameter

REFERENCES

[1] Shaikh, S. R.; Edidin, M. A. Membranes are not just rafts. *Chem. Phys. Lipids*, **2006**, *144* (1), 1-3.

[2] Kusumi, A.; Shirai, Y. M.; Koyama-Honda, I.; Suzuki, K. G.; Fujiwara, T. K. Hierarchical organization of the plasma membrane: investigations by single-molecule tracking vs. fluorescence correlation spectroscopy. *FEBS Lett.*, **2010**, *584* (9), 1814-23.

[3] Lingwood, D.; Simons, K. Lipid rafts as a membrane-organizing principle. *Science*, **2010**, *327* (5961), 46-50.

[4] Lommerse, P. H.; Spaink, H. P.; Schmidt, T. In vivo plasma membrane organization: results of biophysical approaches. *Biochim. Biophys. Acta.*, **2004**, *1664* (2), 119-31.

[5] Edidin, M. The state of lipid rafts: from model membranes to cells. *Annu. Rev. Biophys. Biomol. Struct.*, **2003**, *32*, 257-83.

[6] Anderson, R. G.; Jacobson, K. A role for lipid shells in targeting proteins to caveolae, rafts, and other lipid domains. *Science*, **2002**, *296* (5574), 1821-5.

[7] Jacobson, K.; Mouritsen, O. G.; Anderson, R. G. Lipid rafts: at a crossroad between cell biology and physics. *Nat. Cell Biol.*, **2007**, *9* (1), 7-14.

[8] Kusumi, A.; Nakada, C.; Ritchie, K.; Murase, K.; Suzuki, K.; Murakoshi, H.; Kasai, R. S.; Kondo, J.; Fujiwara, T. Paradigm shift of the plasma membrane concept from the two-dimensional continuum fluid to the partitioned fluid: high-speed single-molecule tracking of membrane molecules. *Annu. Rev. Biophys. Biomol. Struct.*, **2005**, *34*, 351-78.

[9] Engelman, D. M. Membranes are more mosaic than fluid. *Nature*, **2005**, *438* (7068), 578-80.

[10] van Meer, G.; Voelker, D. R.; Feigenson, G. W. Membrane lipids: where they are and how they behave. *Nat. Rev. Mol. Cell Biol.*, **2008**, *9* (2), 112-24.

[11] Wallin, E.; von Heijne, G. Genome-wide analysis of integral membrane proteins from eubacterial, archaean, and eukaryotic organisms. *Protein Sci.*, **1998**, *7* (4), 1029-38.

[12] Mouritsen, O. G. Life - as a matter of fat : the emerging science of lipidomics. Springer: Berlin, 2005; p xii, 276 p.

[13] Galla, H. J.; Hartmann, W.; Theilen, U.; Sackmann, E. On two-dimensional passive random walk in lipid bilayers and fluid pathways in biomembranes. *J. Membr. Biol.*, **1979**, *48* (3), 215-36.

[14] Gudmand, M.; Fidorra, M.; Bjornholm, T.; Heimburg, T. Diffusion and partitioning of fluorescent lipid probes in phospholipid monolayers. *Biophys. J.*, **2009**, *96* (11), 4598-609.

[15] Javanainen, M.; Monticelli, L.; Bernardino de la Serna, J.; Vattulainen, I. Free volume theory applied to lateral diffusion in Langmuir monolayers: atomistic simulations for a protein-free model of lung surfactant. *Langmuir*, **2010**, *26* (19), 15436-44.

[16] Saffman, P. G.; Delbruck, M. Brownian motion in biological membranes. *Proc. Natl. Acad. Sci. USA.*, **1975,** *72* (8), 3111-3.

[17] Singer, S. J.; Nicolson, G. L. The fluid mosaic model of the structure of cell membranes. *Science*, **1972**, *175* (23), 720-31.

[18] Peters, R.; Cherry, R. J. Lateral and rotational diffusion of bacteriorhodopsin in lipid bilayers: experimental test of the Saffman-Delbruck equations. *Proc. Natl. Acad. Sci. USA.,* **1982**, *79* (14), 4317-21.

[19] Ramadurai, S.; Holt, A.; Krasnikov, V.; van den Bogaart, G.; Killian, J. A.; Poolman, B. Lateral diffusion of membrane proteins. *J. Am. Chem. Soc.*, **2009**, *131* (35), 12650-6.

[20] Hughes, B. D.; Pailthorpe, B. A.; White, L. R. The Translational and Rotational Drag on a Cylinder Moving in a Membrane. *J. Fluid. Mech.*, **1981**, *110* (Sep), 349-372.

[21] Hughes, B. D.; Pailthorpe, B. A.; White, L. R.; Sawyer, W. H. Extraction of membrane microviscosity from translational and rotational diffusion coefficients. *Biophys. J.*, **1982**, *37* (3), 673-6.

[22] Petrov, E. P.; Schwille, P. Translational diffusion in lipid membranes beyond the Saffman-Delbruck approximation. *Biophys. J.*, **2008**, *94* (5), L41-3.

[23] Gambin, Y.; Lopez-Esparza, R.; Reffay, M.; Sierecki, E.; Gov, N. S.; Genest, M.; Hodges, R. S.; Urbach, W. Lateral mobility of proteins in liquid membranes revisited. *Proc. Natl. Acad. Sci. USA* **2006**, *103* (7), 2098-102.

[24] Lee, C. C.; Revington, M.; Dunn, S. D.; Petersen, N. O. The lateral diffusion of selectively aggregated peptides in giant unilamellar vesicles. *Biophys. J.*, **2003**, *84* (3), 1756-64.

[25] Guigas, G.; Weiss, M., Size-dependent diffusion of membrane inclusions. *Biophys. J.*, **2006**, *91* (7), 2393-8.

[26] Machan, R.; Hof, M. Lipid diffusion in planar membranes investigated by fluorescence correlation spectroscopy. *Biochim. Biophys. Acta.*, **2010**, *1798* (7), 1377-91.

[27] Przybylo, M.; Sykora, J.; Humpolickova, J.; Benda, A.; Zan, A.; Hof, M. Lipid diffusion in giant unilamellar vesicles is more than 2 times faster than in supported phospholipid bilayers under identical conditions. *Langmuir*, **2006**, *22* (22), 9096-9.

[28] Renner, L.; Osaki, T.; Chiantia, S.; Schwille, P.; Pompe, T.; Werner, C. Supported lipid bilayers on spacious and pH-responsive polymer cushions with varied hydrophilicity. *J. Phys. Chem. B.*, **2008**, *112* (20), 6373-8.

[29] Bockmann, R. A.; Hac, A.; Heimburg, T.; Grubmuller, H. Effect of sodium chloride on a lipid bilayer. *Biophys. J.*, **2003**, *85* (3), 1647-55.

[30] van den Bogaart, G.; Hermans, N.; Krasnikov, V.; de Vries, A. H.; Poolman, B. On the decrease in lateral mobility of phospholipids by sugars. *Biophys. J.*, **2007**, *92* (5), 1598-605.

[31] Vaz, W. L. C.; Goodsaid-Zalduondo, F.; Jacobson, K. Lateral diffusion of lipids and proteins in bilayer membranes. *FEBS Lett.*, **1984**, *174* (2), 199-207.

[32] Chiantia, S.; Ries, J.; Kahya, N.; Schwille, P. Combined AFM and two-focus SFCS study of raft-exhibiting model membranes. *Chemphyschem*, **2006**, *7* (11), 2409-18.

[33] Dietrich, C.; Bagatolli, L. A.; Volovyk, Z. N.; Thompson, N. L.; Levi, M.; Jacobson, K.; Gratton, E. Lipid rafts reconstituted in model membranes. *Biophys. J.*, **2001**, *80* (3), 1417-28.

[34] Vaz, W. L.; Criado, M.; Madeira, V. M.; Schoellmann, G.; Jovin, T. M. Size dependence of the translational diffusion of large integral membrane proteins in liquid-crystalline phase lipid bilayers. A study using fluorescence recovery after photobleaching. *Biochemistry*, **1982**, *21* (22), 5608-12.

[35] Vaz, W. L. C.; Derzko, Z. I.; Jacobson, K. A., Photobleaching Measurements of the Lateral Diffusion of Lipids and Proteins in Artificial Phospholipid-Bilayer Membranes. *Cell Surf. Rev.*, **1982**, *8*, 83-135.

[36] Liu, C.; Paprica, A.; Petersen, N. O. Effects of size of macrocyclic polyamides on their rate of diffusion in model membranes. *Biophys. J.*, **1997**, *73* (5), 2580-7.

[37] Webb, W. W.; Barak, L. S.; Tank, D. W.; Wu, E. S. Molecular mobility on the cell surface. *Biochem. Soc. Symp.*, **1981**, (46), 191-205.

[38] Bacia, K.; Scherfeld, D.; Kahya, N.; Schwille, P. Fluorescence correlation spectroscopy relates rafts in model and native membranes. *Biophys. J.*, **2004**, *87* (2), 1034-43.

[39] Saxton, M. J.; Jacobson, K. Single-particle tracking: applications to membrane dynamics. *Annu. Rev. Biophys. Biomol. Struct.*, **1997**, *26*, 373-99.

[40] Owen, D. M.; Williamson, D.; Rentero, C.; Gaus, K. Quantitative microscopy: protein dynamics and membrane organisation. *Traffic*, **2009**, *10* (8), 962-71.

[41] Adler, J.; Shevchuk, A. I.; Novak, P.; Korchev, Y. E.; Parmryd, I. Plasma membrane topography and interpretation of single-particle tracks. *Nat. Methods*, **2010**, *7* (3), 170-1.

[42] Grant, B. D.; Donaldson, J. G. Pathways and mechanisms of endocytic recycling. *Nat. Rev. Mol. Cell Biol.*, **2009,** *10* (9), 597-608.

[43] Steinman, R. M.; Mellman, I. S.; Muller, W. A.; Cohn, Z. A. Endocytosis and the recycling of plasma membrane. *J. Cell Biol.*, **1983**, *96* (1), 1-27.

[44] Chen, Y.; Lagerholm, B. C.; Yang, B.; Jacobson, K. Methods to measure the lateral diffusion of membrane lipids and proteins. *Methods*, **2006**, *39* (2), 147-53.

[45] Ries, J.; Schwille, P. New concepts for fluorescence correlation spectroscopy on membranes. *Phys. Chem. Chem. Phys.*, **2008**, *10* (24), 3487-97.

[46] Chiantia, S.; Ries, J.; Schwille, P. Fluorescence correlation spectroscopy in membrane structure elucidation. *Biochim. Biophys. Acta.*, **2009**, *1788* (1), 225-33.

[47] Wieser, S.; Schutz, G. J. Tracking single molecules in the live cell plasma membrane-Do's and Don't's. *Methods*, **2008**, *46* (2), 131-40.

[48] Brameshuber, M.; Schutz, G. J. How the sum of its parts gets greater than the whole. *Nat. Methods*, **2008**, *5* (2), 133-4.

[49] Bannai, H.; Levi, S.; Schweizer, C.; Dahan, M.; Triller, A. Imaging the lateral diffusion of membrane molecules with quantum dots. *Nat. Protoc.*, **2006**, *1* (6), 2628-34.

[50] Ram, S.; Prabhat, P.; Chao, J.; Ward, E. S.; Ober, R. J. High accuracy 3D quantum dot tracking with multifocal plane microscopy for the study of fast intracellular dynamics in live cells. *Biophys. J.*, **2008**, *95* (12), 6025-43.

[51] Alcor, D.; Gouzer, G.; Triller, A. Single-particle tracking methods for the study of membrane receptors dynamics. *Eur. J. Neurosci.*, **2009**, *30* (6), 987-97.

[52] Jaqaman, K.; Loerke, D.; Mettlen, M.; Kuwata, H.; Grinstein, S.; Schmid, S. L.; Danuser, G. Robust single-particle tracking in live-cell time-lapse sequences. *Nat. Methods*, **2008**, *5* (8), 695-702.

[53] Serge, A.; Bertaux, N.; Rigneault, H.; Marguet, D. Dynamic multiple-target tracing to probe spatiotemporal cartography of cell membranes. *Nat. Methods*, **2008**, *5* (8), 687-94.

[54] Pinaud, F.; Michalet, X.; Iyer, G.; Margeat, E.; Moore, H. P.; Weiss, S. Dynamic partitioning of a glycosyl-phosphatidylinositol-anchored protein in glycosphingolipid-rich microdomains imaged by single-quantum dot tracking. *Traffic*, **2009**, *10* (6), 691-712.

[55] Schutz, G. J.; Schindler, H.; Schmidt, T. Single-molecule microscopy on model membranes reveals anomalous diffusion. *Biophys. J.*, **1997**, *73* (2), 1073-80.

[56] Qian, H.; Sheetz, M. P.; Elson, E. L. Single particle tracking. Analysis of diffusion and flow in two-dimensional systems. *Biophys. J.*, **1991**, *60* (4), 910-21.

[57] Hink, M. A.; Griep, R. A.; Borst, J. W.; van Hoek, A.; Eppink, M. H.; Schots, A.; Visser, A. J. Structural dynamics of green fluorescent protein alone and fused with a single chain Fv protein. *J. Biol. Chem.*, **2000**, *275* (23), 17556-60.

[58] Lagerholm, B. C.; Weinreb, G. E.; Jacobson, K.; Thompson, N. L. Detecting microdomains in intact cell membranes. *Annu. Rev. Phys. Chem.*, **2005**, *56*, 309-36.

[59] Chen, I.; Ting, A. Y. Site-specific labeling of proteins with small molecules in live cells. *Curr. Opin. Biotechnol.*, **2005**, *16* (1), 35-40.

[60] Chen, I.; Howarth, M.; Lin, W.; Ting, A. Y. Site-specific labeling of cell surface proteins with biophysical probes using biotin ligase. *Nat. Methods*, **2005**, *2* (2), 99-104.

[61] Johnsson, N.; George, N.; Johnsson, K. Protein chemistry on the surface of living cells. *Chembiochem.*, **2005**, *6* (1), 47-52.

[62] Keppler, A.; Gendreizig, S.; Gronemeyer, T.; Pick, H.; Vogel, H.; Johnsson, K. A general method for the covalent labeling of fusion proteins with small molecules in vivo. *Nat. Biotechnol.*, **2003**, *21* (1), 86-9.

[63] Griffin, B. A.; Adams, S. R.; Tsien, R. Y. Specific covalent labeling of recombinant protein molecules inside live cells. *Science*, **1998**, *281* (5374), 269-72.

[64] Yu, C.; Hale, J.; Ritchie, K.; Prasad, N. K.; Irudayaraj, J. Receptor overexpression or inhibition alters cell surface dynamics of EGF-EGFR interaction: new insights from real-time single molecule analysis. *Biochem. Biophys. Res. Commun.*, **2009**, *378* (3), 376-82.

[65] Howarth, M.; Chinnapen, D. J.; Gerrow, K.; Dorrestein, P. C.; Grandy, M. R.; Kelleher, N. L.; El-Husseini, A.; Ting, A. Y. A monovalent streptavidin with a single femtomolar biotin binding site. *Nat. Methods*, **2006**, *3* (4), 267-73.

[66] You, C.; Wilmes, S.; Beutel, O.; Lochte, S.; Podoplelowa, Y.; Roder, F.; Richter, C.; Seine, T.; Schaible, D.; Uze, G.; Clarke, S.; Pinaud, F.; Dahan, M.; Piehler, J. Self-controlled monofunctionalization of quantum dots for multiplexed protein tracking in live cells. *Angew. Chem. Int. Ed. Engl.*, **2010**, *49* (24), 4108-12.

[67] Howarth, M.; Liu, W.; Puthenveetil, S.; Zheng, Y.; Marshall, L. F.; Schmidt, M. M.; Wittrup, K. D.; Bawendi, M. G.; Ting, A. Y., Monovalent, reduced-size quantum dots for imaging receptors on living cells. *Nat Methods* **2008,** *5* (5), 397-9.

[68] Clarke, S.; Pinaud, F.; Beutel, O.; You, C.; Piehler, J.; Dahan, M., Covalent monofunctionalization of peptide-coated quantum dots for single-molecule assays. *Nano Lett* **2010,** *10* (6), 2147-54.

[69] Sperling, R. A.; Pellegrino, T.; Li, J. K.; Chang, W. H.; Parak, W. J. Electrophoretic separation of nanoparticles with a discrete number of functional groups. *Adv. Func. Mat.*, **2006**, *16* (7), 943-948.

[70] Zanchet, D.; Micheel, C. M.; Parak, W. J.; Gerion, D.; Alivisatos, A. P. Electrophoretic Isolation of Discrete Au Nanocrystal/DNA Conjugates. *Nano. Letts.*, **2000**, *1* (1), 32-35.

[71] Wustner, D. Fluorescent sterols as tools in membrane biophysics and cell biology. *Chem. Phys. Lipids*, **2007**, *146* (1), 1-25.

[72] Sosinsky, G. E.; Gaietta, G. M.; Hand, G.; Deerinck, T. J.; Han, A.; Mackey, M.; Adams, S. R.; Bouwer, J.; Tsien, R. Y.; Ellisman, M. H. Tetracysteine genetic tags complexed with biarsenical ligands as a tool for investigating gap junction structure and dynamics. *Cell Commun. Adhes.*, **2003**, *10* (4-6), 181-6.

[73] Wieser, S.; Moertelmaier, M.; Fuertbauer, E.; Stockinger, H.; Schutz, G. J. (Un)confined diffusion of CD59 in the plasma membrane determined by high-resolution single molecule microscopy. *Biophys. J.*, **2007**, *92* (10), 3719-28.

[74] Espenel, C.; Margeat, E.; Dosset, P.; Arduise, C.; Le Grimellec, C.; Royer, C. A.; Boucheix, C.; Rubinstein, E.; Milhiet, P. E. Single-molecule analysis of CD9 dynamics and partitioning reveals multiple modes of interaction in the tetraspanin web. *J. Cell Biol.*, **2008**, *182* (4), 765-76.

[75] Giepmans, B. N.; Adams, S. R.; Ellisman, M. H.; Tsien, R. Y. The fluorescent toolbox for assessing protein location and function. *Science*, **2006**, *312* (5771), 217-24.

[76] Lommerse, P. H. M.; Vastenhoud, K.; Pirinen, N. J.; Magee, A. I.; Spaink, H. P.; Schmidt, T. Single-molecule diffusion reveals similar mobility for the Lck, H-Ras, and K-Ras membrane anchors. *Biophys. J.*, **2006**, *91* (3), 1090-1097.

[77] Sunbul, M.; Yen, M.; Zou, Y.; Yin, J. Enzyme catalyzed site-specific protein labeling and cell imaging with quantum dots. *Chem. Commun. (Camb.)*, **2008**, (45), 5927-9.

[78] Chakraborty, S. K.; Fitzpatrick, J. A.; Phillippi, J. A.; Andreko, S.; Waggoner, A. S.; Bruchez, M. P.; Ballou, B. Cholera toxin B conjugated quantum dots for live cell labeling. *Nano. Lett.*, **2007**, *7* (9), 2618-26.

[79] Durisic, N.; Bachir, A. I.; Kolin, D. L.; Hebert, B.; Lagerholm, B. C.; Grutter, P.; Wiseman, P. W. Detection and correction of blinking bias in image correlation transport measurements of quantum dot tagged macromolecules. *Biophys. J.*, **2007**, *93* (4), 1338-46.

[80] Groc, L.; Heine, M.; Cognet, L.; Brickley, K.; Stephenson, F. A.; Lounis, B.; Choquet, D. Differential activity-dependent regulation of the lateral mobilities of AMPA and NMDA receptors. *Nat. Neurosci.*, **2004**, *7* (7), 695-6.

[81] Hohng, S.; Ha, T. Near-complete suppression of quantum dot blinking in ambient conditions. *J. Am. Chem. Soc.*, **2004**, *126* (5), 1324-5.

[82] Andrews, N. L.; Lidke, K. A.; Pfeiffer, J. R.; Burns, A. R.; Wilson, B. S.; Oliver, J. M.; Lidke, D. S. Actin restricts FcepsilonRI diffusion and facilitates antigen-induced receptor immobilization. *Nat. Cell Biol.*, **2008**, *10* (8), 955-63.

[83] Pons, T.; Mattoussi, H. Investigating biological processes at the single molecule level using luminescent quantum dots. *Ann. Biomed. Eng.*, **2009**, *37* (10), 1934-59.

[84] Michalet, X.; Pinaud, F.; Lacoste, T. D.; Dahan, M.; Bruchez, M. P.; Alivisatos, A. P.; Weiss, S. Properties of fluorescent semiconductor nanocrystals and their application to biological labeling. *Single Mol.*, **2001**, *2* (4), 261-276.

[85] Bruchez, M., Jr.; Moronne, M.; Gin, P.; Weiss, S.; Alivisatos, A. P. Semiconductor nanocrystals as fluorescent biological labels. *Science*, **1998**, *281* (5385), 2013-6.

[86] Wu, X.; Liu, H.; Liu, J.; Haley, K. N.; Treadway, J. A.; Larson, J. P.; Ge, N.; Peale, F.; Bruchez, M. P. Immunofluorescent labeling of cancer marker Her2 and other cellular targets with semiconductor quantum dots. *Nat. Biotechnol.*, **2003**, *21* (1), 41-6.

[87] Fujiwara, T.; Ritchie, K.; Murakoshi, H.; Jacobson, K.; Kusumi, A. Phospholipids undergo hop diffusion in compartmentalized cell membrane. *J. Cell Biol.*, **2002**, *157* (6), 1071-81.

[88] Wong, S. F.; Meng, C. K.; Fenn, J. B. Multiple Charging in Electrospray Ionization of Poly(Ethylene Glycols). *J. Phys. Chem-Us.*, **1988**, *92* (2), 546-550.

[89] Umemura, Y. M.; Vrljic, M.; Nishimura, S. Y.; Fujiwara, T. K.; Suzuki, K. G.; Kusumi, A. Both MHC class II and its GPI-anchored form undergo hop diffusion as observed by single-molecule tracking. *Biophys. J.*, **2008**, *95* (1), 435-50.

[90] Sheets, E. D.; Lee, G. M.; Simson, R.; Jacobson, K. Transient confinement of a glycosylphosphatidylinositol-anchored protein in the plasma membrane. *Biochemistry*, **1997**, *36* (41), 12449-58.

[91] Suzuki, K. G.; Fujiwara, T. K.; Edidin, M.; Kusumi, A. Dynamic recruitment of phospholipase C gamma at transiently immobilized GPI-anchored receptor clusters induces IP3-Ca2+ signaling: single-molecule tracking study 2. *J. Cell Biol.*, **2007**, *177* (4), 731-42.

[92] Chen, Y.; Thelin, W. R.; Yang, B.; Milgram, S. L.; Jacobson, K. Transient anchorage of cross-linked glycosyl-phosphatidylinositol-anchored proteins depends on cholesterol, Src family kinases, caveolin, and phosphoinositides. *J. Cell Biol.*, **2006**, *175* (1), 169-78.

[93] Suzuki, K.; Ritchie, K.; Kajikawa, E.; Fujiwara, T.; Kusumi, A. Rapid hop diffusion of a G-protein-coupled receptor in the plasma membrane as revealed by single-molecule techniques. *Biophys. J.*, **2005**, *88* (5), 3659-80.

[94] Simson, R.; Sheets, E. D.; Jacobson, K. Detection of temporary lateral confinement of membrane proteins using single-particle tracking analysis. *Biophys. J.*, **1995**, *69* (3), 989-93.

[95] Murcia, M. J.; Minner, D. E.; Mustata, G. M.; Ritchie, K.; Naumann, C. A. Design of quantum dot-conjugated lipids for long-term, high-speed tracking experiments on cell surfaces. *J. Am. Chem. Soc.*, **2008**, *130* (45), 15054-62.

[96] Dietrich, C.; Yang, B.; Fujiwara, T.; Kusumi, A.; Jacobson, K. Relationship of lipid rafts to transient confinement zones detected by single particle tracking. *Biophys. J.*, **2002**, *82* (1 Pt 1), 274-84.

[97] Kenworthy, A. K.; Nichols, B. J.; Remmert, C. L.; Hendrix, G. M.; Kumar, M.; Zimmerberg, J.; Lippincott-Schwartz, J. Dynamics of putative raft-associated proteins at the cell surface. *J. Cell Biol.*, **2004**, *165* (5), 735-46.

[98] Rhode, S.; Grurl, R.; Brameshuber, M.; Hermetter, A.; Schutz, G. J. Plasma membrane fluidity affects transient immobilization of oxidized phospholipids in endocytotic sites for subsequent uptake. *J. Biol. Chem.*, **2009**, *284* (4), 2258-65.

[99] Lommerse, P. H.; Vastenhoud, K.; Pirinen, N. J.; Magee, A. I.; Spaink, H. P.; Schmidt, T. Single-molecule diffusion reveals similar mobility for the Lck, H-ras, and K-ras membrane anchors. *Biophys. J.*, **2006**, *91* (3), 1090-7.

[100] Murase, K.; Fujiwara, T.; Umemura, Y.; Suzuki, K.; Iino, R.; Yamashita, H.; Saito, M.; Murakoshi, H.; Ritchie, K.; Kusumi, A. Ultrafine membrane compartments for molecular diffusion as revealed by single molecule techniques. *Biophys. J.*, **2004**, *86* (6), 4075-93.

[101] Suzuki, K. G.; Fujiwara, T. K.; Sanematsu, F.; Iino, R.; Edidin, M.; Kusumi, A. GPI-anchored receptor clusters transiently recruit Lyn and G alpha for temporary cluster immobilization and Lyn activation: single-molecule tracking study 1. *J. Cell Biol.*, **2007**, *177* (4), 717-30.

[102] Morone, N.; Fujiwara, T.; Murase, K.; Kasai, R. S.; Ike, H.; Yuasa, S.; Usukura, J.; Kusumi, A. Three-dimensional reconstruction of the membrane skeleton at the plasma membrane interface by electron tomography. *J. Cell Biol.*, **2006**, *174* (6), 851-62.

[103] Malorni, W.; Testa, U.; Rainaldi, G.; Tritarelli, E.; Peschle, C. Oxidative stress leads to a rapid alteration of transferrin receptor intravesicular trafficking. *Exp. Cell Res.*, **1998**, *241* (1), 102-16.

[104] Frick, M.; Schmidt, K.; Nichols, B. J. Modulation of lateral diffusion in the plasma membrane by protein density. *Curr. Biol.*, **2007**, *17* (5), 462-7.

[105] Chen, Y.; Yang, B.; Jacobson, K. Transient confinement zones: a type of lipid raft? *Lipids,* **2004**, *39* (11), 1115-9.

[106] Kusumi, A.; Koyama-Honda, I.; Suzuki, K. Molecular dynamics and interactions for creation of stimulation-induced stabilized rafts from small unstable steady-state rafts. *Traffic*, **2004**, *5* (4), 213-30.

[107] Chen, H.; Titushkin, I.; Stroscio, M.; Cho, M. Altered membrane dynamics of quantum dot-conjugated integrins during osteogenic differentiation of human bone marrow derived progenitor cells. *Biophys. J.*, **2007**, *92* (4), 1399-408.

[108] Bates, I. R.; Hebert, B.; Luo, Y.; Liao, J.; Bachir, A. I.; Kolin, D. L.; Wiseman, P. W.; Hanrahan, J. W. Membrane lateral diffusion and capture of CFTR within transient confinement zones. *Biophys. J.*, **2006**, *91* (3), 1046-58.

[109] Haggie, P. M.; Kim, J. K.; Lukacs, G. L.; Verkman, A. S. Tracking of quantum dot-labeled CFTR shows near immobilization by C-terminal PDZ interactions. *Mol. Biol. Cell.*, **2006**, *17* (12), 4937-45.

[110] Thelin, W. R.; Chen, Y.; Gentzsch, M.; Kreda, S. M.; Sallee, J. L.; Scarlett, C. O.; Borchers, C. H.; Jacobson, K.; Stutts, M. J.; Milgram, S. L. Direct interaction with filamins modulates the stability and plasma membrane expression of CFTR. *J. Clin. Invest.*, **2007**, *117* (2), 364-74.

[111] Lidke, D. S.; Lidke, K. A.; Rieger, B.; Jovin, T. M.; Arndt-Jovin, D. J. Reaching out for signals: filopodia sense EGF and respond by directed retrograde transport of activated receptors. *J. Cell Biol.*, **2005**, *170* (4), 619-26.

[112] Lidke, D. S.; Nagy, P.; Heintzmann, R.; Arndt-Jovin, D. J.; Post, J. N.; Grecco, H. E.; Jares-Erijman, E. A.; Jovin, T. M. Quantum dot ligands provide new insights into erbB/HER receptor-mediated signal transduction. *Nat. Biotechnol.*, **2004**, *22* (2), 198-203.

[113] Kodippili, G. C.; Spector, J.; Sullivan, C.; Kuypers, F. A.; Labotka, R.; Gallagher, P. G.; Ritchie, K.; Low, P. S. Imaging of the diffusion of single band 3 molecules on normal and mutant erythrocytes. *Blood*, **2009**, *113* (24), 6237-45.

[114] Rust, M. J.; Bates, M.; Zhuang, X. Sub-diffraction-limit imaging by stochastic optical reconstruction microscopy (STORM). *Nat. Methods*, **2006**, *3* (10), 793-5.

[115] Betzig, E.; Patterson, G. H.; Sougrat, R.; Lindwasser, O. W.; Olenych, S.; Bonifacino, J. S.; Davidson, M. W.; Lippincott-Schwartz, J.; Hess, H. F. Imaging intracellular fluorescent proteins at nanometer resolution. *Science*, **2006**, *313* (5793), 1642-5.

[116] Manley, S.; Gillette, J. M.; Patterson, G. H.; Shroff, H.; Hess, H. F.; Betzig, E.; Lippincott-Schwartz, J. High-density mapping of single-molecule trajectories with photoactivated localization microscopy. *Nat. Methods*, **2008**, *5* (2), 155-7.

[117] Eggeling, C.; Ringemann, C.; Medda, R.; Schwarzmann, G.; Sandhoff, K.; Polyakova, S.; Belov, V. N.; Hein, B.; von Middendorff, C.; Schonle, A.; Hell, S. W. Direct observation of the nanoscale dynamics of membrane lipids in a living cell. *Nature*, **2009**, *457* (7233), 1159-62.

[118] Sahl, S. J.; Leutenegger, M.; Hilbert, M.; Hell, S. W.; Eggeling, C., Fast molecular tracking maps nanoscale dynamics of plasma membrane lipids. *Proc. Natl. Acad. Sci. USA*, **2010**, *107* (15), 6829-34.

[119] Lajoie, P.; Partridge, E. A.; Guay, G.; Goetz, J. G.; Pawling, J.; Lagana, A.; Joshi, B.; Dennis, J. W.; Nabi, I. R. Plasma membrane domain organization regulates EGFR signaling in tumor cells. *J. Cell Biol.*, **2007**, *179* (2), 341-56.

[120] Wymann, M. P.; Schneiter, R. Lipid signalling in disease. *Nat. Rev. Mol. Cell Biol.*, **2008**, *9* (2), 162-76.

[121] Baumgart, T.; Hammond, A. T.; Sengupta, P.; Hess, S. T.; Holowka, D. A.; Baird, B. A.; Webb, W. W. Large-scale fluid/fluid phase separation of proteins and lipids in giant plasma membrane vesicles. *Proc. Natl. Acad. Sci. USA*, **2007**, *104* (9), 3165-70.

[122] Lingwood, D.; Ries, J.; Schwille, P.; Simons, K. Plasma membranes are poised for activation of raft phase coalescence at physiological temperature. *Proc. Natl. Acad. Sci. USA*, **2008**, *105* (29), 10005-10.

[123] Armstrong, J. K.; Wenby, R. B.; Meiselman, H. J.; Fisher, T. C. The hydrodynamic radii of macromolecules and their effect on red blood cell aggregation. *Biophys. J.*, **2004**, *87* (6), 4259-70.

Received: September 29, 2010 Revised: January 25, 2011 Accepted: January 27, 2011